Brownian dynamics study of the influences of electrostatic interaction and diffusion on protein–protein association kinetics

Huan-Xiang Zhou
National Institute of Diabetes and Digestive and Kidney Diseases, National Institutes of Health, Bethesda, Maryland 20892 USA

ABSTRACT A unified model is presented for protein–protein association processes that are under the influences of electrostatic interaction and diffusion (e.g., protein oligomerization, enzyme catalysis, electron and energy transfer). The proteins are modeled as spheres that bear point charges and undergo translational and rotational Brownian motion. Before association can occur the two spheres have to be aligned properly to form a reaction complex via diffusion. The reaction complex can either go on to form the product or it can dissociate into the separate reactants through diffusion. The electrostatic interaction, like diffusion, influences every step except the one that brings the reaction complex into the product. The interaction potential is obtained by extending the Kirkwood–Tanford protein model (Tanford, C., and J. G. Kirkwood. 1957. *J. Am. Chem. Soc.* 79:5333–5339) to two charge-embedded spheres and solving the consequent equations under a particular basis set. The time-dependent association rate coefficient is then obtained through Brownian dynamics simulations according an algorithm developed earlier (Zhou, H.-X. 1990. *J. Phys. Chem.* 94:8794–8800). This method is applied to a model system of the cytochrome *c* and cytochrome *c* peroxidase association process and the results confirm the experimental dependence of the association rate constant on the solution ionic strength. An important conclusion drawn from this study is that when the product is formed by very specific alignment of the reactants, as is often the case, the effect of the interaction potential is simply to scale the association rate constant by a Boltzmann factor. This explains why mutations in the interface of the reaction complex have strong influences on the association rate constant whereas those away from the interface have minimal effects. It comes about because the former mutations change the interaction potential of the reaction complex significantly and the latter ones do not.

INTRODUCTION

In this paper we present a unified model for protein–protein association processes that are under the influences of electrostatic interaction and diffusion (e.g., protein oligomerization, enzyme catalysis, electron and energy transfer). The proteins are modeled as spheres that bear point charges and undergo translational and rotational Brownian motion.

Electrostatic interaction plays a prominent role in diffusion-influenced reactions. After the classical work of Smoluchowski (1) that calculated the association rate constant of two isotropically reactive spheres, the next significant step came when Debye (2) included the effect of the electrostatic interaction between the spheres on the association rate constant. Debye considered the simple charge–charge Coulombic interaction and the interaction discussed earlier by Debye and Huckel (3) between a test charge and a sphere bearing a central charge in ionic solutions. Recent advancement was made by Sharp et al. (4), who first put the electrostatic field calculated numerically from the Poisson–Boltzmann equation into the newly developed algorithm of Northrup et al. (5) for calculating diffusion-influenced reaction rates through Brownian dynamics simulations. The method of solving the Poisson–Boltzmann equation originates from the work of Warwicker and Watson (6), who applied finite differences to the problem of electrostatics around an irregular cavity. Developments along this line are summarized in the review of Davis and McCammon (7). Among the most sophisticated in these developments is the work of Northrup et al. (8), who studied the diffusional association of electron-transfer proteins cytochrome *c* and cytochrome *c* peroxidase. It should be noted that even in this work cytochrome *c* was treated differently from cytochrome *c* peroxidase, i.e., as a collection of test charges rather than a low dielectric region that excludes ions. This treatment of cytochrome *c* changes the interaction potential significantly, as will be seen later in this paper.

In this paper we treat the associating proteins on equal footing. The first such treatment was perhaps that of Scatchard and Kirkwood (9). They worked out the first few terms of the expansion of the electrostatic potential in spherical harmonics and their contributions to the free energy for a simple model. The model consists of two symmetric spheres bearing central charges immersed in an ionic solution. Kirkwood later abandoned this approach because of the mathematical complexity involved. Instead he (10) went on to treat a single sphere bearing an arbitrary distribution of point charges. This method was later applied to proteins to determine protein titration curves by Tanford and Kirkwood (11). More recent extensions of the Tanford–Kirkwood protein model include an ad hoc method introduced by Shire et al. (12) for accounting the irregular shape of the protein using a scaling factor that depends on the solvent accessibility of each charged residue. Developments along this line are reviewed by Matthew (13). We note again that even in cases involving two proteins calculations were based on a single charge-bearing sphere (14).

A single sphere is inadequate in modeling a protein–protein complex, and even more so in studying the association process. In this process most of the time the two proteins are far apart and separated by the solvent. Consequently in this paper we take up the original Scatchard

and Kirkwood (9) approach and model the two proteins as separate charge-bearing spheres. As a result we obtain an infinite set of linear equations. We solve them by truncating at appropriate orders. Their solution provides the interaction potential between the two proteins. We then put this interaction potential into the algorithm developed earlier (15) for calculating the time-dependent rate coefficient of diffusion-influenced reactions using Brownian dynamics simulations. This combination yields the following model for diffusion-influenced protein–protein association. The charge-bearing spheres modeling the proteins undergo translational and rotational Brownian motion. Before association can occur, the two spheres have to be aligned properly to form a reaction complex via diffusion. The reaction complex can either go on to form the product or it can dissociate into the separate reactants through diffusion. The electrostatic interaction, like diffusion, influences every step except the one that brings the reaction complex into the product. We will apply this method to a model system of the cytochrome *c* and cytochrome *c* peroxidase association process and compare the results with the experimental dependence of the association rate constant on the solution ionic strength.

The rest of the paper is organized as follows. First we introduce our protein–protein association model under a simpler situation where the interaction potential is centrosymmetric and the reaction complex is formed only when the spheres are at contact and the contact point is within certain surface patches of the respective spheres. This situation has further significance in that it is perhaps the most general one for which an analytical solution of the time-dependent rate coefficient can be achieved. This we obtain by using the constant-flux approximation introduced by Shoup et al. (16). Its simplifications in various cases are compared with earlier results (16–21). A remarkable result emerges from this derivation. When the reactive patches that lead to the reaction complex on one or both spheres are small, the effect of the interaction potential is simply to scale the association rate constant by the Boltzmann factor of the contact potential.

We then describe the method for calculating the interaction potential for two spheres bearing arbitrary distributions of point charges and immersed in a salt solution. It is next applied to the diffusional association of a model system of cytochrome *c* and cytochrome *c* peroxidase introduced by Northrup et al. (22). In this model each protein bears three charges. Using Brownian dynamics simulations we calculate the time-dependent rate coefficient of the system under three ionic strengths and in the absence of the electrostatic potential. The dependence of the steady-state association rate constant on the solution ionic strength is compared with experiments (23), and close agreement is obtained. Furthermore, when the association rate constant in the presence and absence of the interaction potential are compared, a result similar to what is in the case of a centrosymmetric potential is found. In cases in which the reactive patches are small, the effect of the interaction potential is to scale the association rate constant by the Boltzmann factor averaged over all the configurations of the reaction complex. This result allows ready estimate of the association rate constant when a different potential field is present.

The final section of the paper summarizes the results of this study and discusses their consequences and implications. In particular, we show that charge mutations near the reactive patches significantly change the contact potential and consequently the association rate constant; on the other hand mutations away from the reactive patches have minimal effect.

MODEL UNDER A CENTROSYMMETRIC INTERACTION POTENTIAL

In this section we describe and solve our general protein–protein diffusional association model under a simpler situation. The simplification is twofold. The interaction potential depends only on the interprotein distance and not on the orientations of the two spheres or the orientation of their displacement vector. Additionally, rather than having an arbitrary configuration space, the reaction complex is formed when the spheres are at contact and the contact point is within axially symmetric patches covering a portion of their surfaces. It should be emphasized that despite these two restrictions this model extends even the general model of Solc and Stockmayer (17) by allowing for a centrosymmetric interaction potential. Below we obtain an analytical solution for the time-dependent rate coefficient of this model. This is accomplished by using the constant-flux approximation introduced by Shoup et al. (16).

The configuration of the system is specified by the displacement vector $\mathbf{r} = r\mathbf{e}$ between the two spheres and the unit vectors $\mathbf{e}_1$ and $\mathbf{e}_2$ along the symmetry axes of their reactive patches (Fig. 1). The distribution function in this space at time t, $P(r\mathbf{e}, \mathbf{e}_1, \mathbf{e}_2, t)$, satisfies the diffusion equation

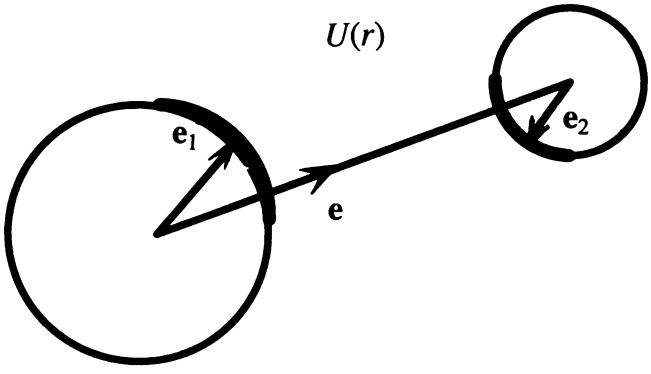

FIGURE 1 The system of two patched spheres under the influence of a centrosymmetric interaction potential.

$$\frac{\partial P}{\partial t} = \mathcal{L}_{tr} P, \tag{1a}$$

$$\mathcal{L}_{tr} = D\nabla \cdot e^{-\beta U(r)} \nabla e^{\beta U(r)} + \sum_{i=1}^{2} D_i \Omega_i \cdot \Omega_i$$

$$= D\mathcal{L}(r) + \frac{D}{r^2} \mathscr{H}(\mathbf{e}) + \sum_{i=1}^{2} D_i \mathscr{H}(\mathbf{e}_i). \tag{1b}$$

In the above equation D is the relative translational diffusion constant, i.e., the sum of the translational diffusion constants of the two spheres, and D_i is the rotational diffusion constant of the ith sphere. $\nabla = \partial/\partial \mathbf{r}$ is the gradient operator, and $\Omega_i = \mathbf{e}_i \times \partial/\partial \mathbf{e}_i$ are angular gradient operators. The radial part of the translational diffusion operator is

$$\mathcal{L}(r) = \frac{1}{r^2} \frac{\partial}{\partial r} r^2 e^{-\beta U(r)} \frac{\partial}{\partial r} e^{\beta U(r)}, \tag{2a}$$

where $\beta = (k_B T)^{-1}$ is the inverse of the product of Boltzmann's constant and the absolute temperature, and $U(r)$ is the interaction potential. The rotational diffusion operators as well as the angular part of the translational diffusion operator are

$$\mathscr{H}(\mathbf{e}) = \frac{1}{\sin\theta} \frac{\partial}{\partial \theta} \sin\theta \frac{\partial}{\partial \theta} + \frac{1}{\sin^2\theta} \frac{\partial^2}{\partial^2 r}, \tag{2b}$$

where (θ, ϕ) expresses $\mathbf{e}$ (similarly for $\mathbf{e}_1$ and $\mathbf{e}_2$) in spherical coordinates. When the two spheres are at contact, i.e., when $r = a_1 + a_2 \equiv a$ (a_i: radius of the ith sphere), the distribution function $P(r\mathbf{e}, \mathbf{e}_1, \mathbf{e}_2, t)$ satisfies the following radiation-type boundary condition:

$$De^{-\beta U(r)} \frac{\partial}{\partial r} e^{\beta U(r)} P = \kappa u_1(\gamma_1) u_2(\gamma_2) P, \quad r = a. \tag{3}$$

In the above $u_i(\gamma_i)$ is some step function that is 1 over certain range of γ_i and zero elsewhere, whereas γ_1 and γ_2 are the angles between the contact point and the vectors $\mathbf{e}_1$ and $\mathbf{e}_2$, respectively. They are given by

$$\cos\gamma_1 = \cos\theta\cos\theta_1 + \sin\theta\sin\theta_1\cos(\phi - \phi_1), \tag{4a}$$

$$\cos(\pi - \gamma_2) = \cos\theta\cos\theta_2 + \sin\theta\sin\theta_2\cos(\phi - \phi_2). \tag{4b}$$

The above prescription extends the general model of Solc and Stockmayer (17) by including a centrosymmetric interaction potential $U(r)$. The time-dependent rate coefficient of this model is the total flux across the boundary $r = a$,

$$k(t) = Da^2 \iiint d\mathbf{e}\, d\mathbf{e}_1\, d\mathbf{e}_2 \Big[e^{-\beta U(r)} \frac{\partial}{\partial r} e^{\beta U(r)} \times P(r\mathbf{e}, \mathbf{e}_1, \mathbf{e}_2, t) \Big]_{r=a} \tag{5a}$$

$$= \kappa a^2 \iiint d\mathbf{e}\, d\mathbf{e}_1\, d\mathbf{e}_2 u_1(\gamma_1) u_2(\gamma_2) \times P(a\mathbf{e}, \mathbf{e}_1, \mathbf{e}_2, t). \tag{5b}$$

Its Laplace transform, $\hat{k}(s)$, can be obtained by using the constant-flux approximation. In this approximation the flux is assumed to be a constant when the contact point is in the reactive patches and this constant is determined by requiring the radiation boundary condition to be satisfied on the average. The details of the derivation are given in Appendix A; the final result is

$$s\hat{k}(s) = \frac{Da^2\kappa e^{-\beta U(a)} [c_1(0)c_2(0)]^2}{4\pi D c_1(0)c_2(0) - \kappa \sum_{l,l_1,l_2=0}^{\infty} \frac{f_l[a; \mu_{l_1 l_2}(s)]}{f_l'[a; \mu_{l_1 l_2}(s)]} [c_1(l_1)c_2(l_2)]^2 C_{l l_1 l_2}}. \tag{6}$$

In the above $\mu_{l_1 l_2}(s) = [(D_1 l_1(l_1 + 1) + D_2 l_2(l_2 + 1) + s)/D]^{1/2}$ and $f_l(r; \mu)$ are the regular solutions of the equations

$$\left\{ \mathcal{L}^+(r) - \left[\mu^2 + \frac{l(l+1)}{r^2} \right] \right\} f_l \equiv \left\{ \frac{e^{\beta U(r)}}{r^2} \frac{d}{dr} r^2 e^{-\beta U(r)} \frac{d}{dr} - \left[\mu^2 + \frac{l(l+1)}{r^2} \right] \right\} f_l = 0, \tag{7}$$

$c_i(l_i)$ are the expansion coefficients of $u_i(\gamma_i)$ in terms of the Legendre polynomials $P_{l_i}(\cos\gamma_i)$,

$$c_i(l_i) = 2\pi \int_0^{\pi} u_i(\gamma_i) P_{l_i}(\cos\gamma_i) \sin\gamma_i\, d\gamma_i, \tag{8}$$

and $C_{l l_1 l_2}$ are expressions made of 3-j symbols,

$$C_{l l_1 l_2} = \frac{(2l_1 + 1)(2l_2 + 1)(2l + 1)}{4\pi} \begin{pmatrix} l_1 & l_2 & l \\ 0 & 0 & 0 \end{pmatrix}^2. \tag{9}$$

Some general properties of $k(t)$ can be easily obtained from the expression of its Laplace transform, Eq. 6. Its initial value is

$$k(0) = 4\pi\kappa a^2 F_1 F_2 e^{-\beta U(a)}, \tag{10}$$

where $F_i = c_i(0)/4\pi$. This is an expected result; it is just the reactivity κ multiplied by the fractional reactive surface area $4\pi a^2 F_1 F_2$ and the Boltzmann factor of the contact potential. With Eq. 10 we can write $\hat{k}(s)$ in the following form:

$$s\hat{k}(s) = \frac{k(0) s\hat{k}_D(s)}{k(0) + s\hat{k}_D(s)}, \tag{11}$$

where $\hat{k}_D(s)$ is the Laplace transform of $k(t)$ when the reaction is diffusion controlled, i.e., when the reactivity κ is infinite. In fact Eq. 11 is a general relationship between the rate coefficient under finite and infinite reactivities.

The long-time asymptotic behavior of $k(t)$ can be found from the expansion of $\hat{k}(s)$ around $s = 0$. We first observe that in expanding $f_l[a; \mu_{l_1l_2}(s)]/f_l'[a; \mu_{l_1l_2}(s)]$, next to the s^0 order only the $ll_1l_2 = 000$ term contributes to the $s^{1/2}$ order; the rest of the terms start their contributions at the s order. This $s^{1/2}$-order contribution from the $ll_1l_2 = 000$ term can be found from the work of Szabo and Zhou (24, 25); one has

$$-a^2e^{-\beta U(a)}f_0'[a; \mu_{00}(s)]/f_0[a; \mu_{00}(s)] = a_{eff}(1 + a_{eff}\sqrt{s/D} + \cdots), \quad (12a)$$

$$a_{eff} = \left[\int_a^\infty \frac{dr}{r^2}\, e^{\beta U(r)}\right]^{-1}. \quad (12b)$$

Consequently,

$$[s\hat{k}(s)]^{-1} = k(\infty) - \sqrt{z/D}/4\pi D + \cdots, \quad (13)$$

and

$$k(t) = k(\infty)\left(1 + \frac{k(\infty)/4\pi D}{\sqrt{\pi Dt}} + \cdots\right). \quad (14)$$

The steady-state rate constant $k(\infty)$ is given by Eq. 6 with $s = 0$. Eq. 14 belongs to a general form of the asymptotic behavior of $k(t)$.

The case where the interaction potential $U(r) = 0$ has attracted special attention (18, 20, 21). The functions $f_l(r; \mu_{l_1l_2}(s))$ in this case can be solved explicitly. They are just the modified Bessel functions of the third kind,

$$f_l[r; \mu_{l_1l_2}(s)] = \sqrt{\frac{\pi}{2\mu_{l_1l_2}(s)r}}\, K_{l+1/2}[\mu_{l_1l_2}(s)r]. \quad (15)$$

Several approximations for the steady-state rate constant of this case have been obtained previously. Eq. 6 with $s = 0$ and $f_l[r; \mu_{l_1l_2}(s)]$ given by Eq. 15 is equivalent to the result of Temkin and Yakobson (20) using a completely different approach. They obtained $k_D(\infty)$ by finding the mean total residence time of the reaction complex before diffusion brings it apart, calculated from the Green function of the system in the absence of reaction. This approach was originated by Wilemski and Fixman (26) and developed further by Doi (27).

Originally Solc and Stockmayer (18) proposed a quasichemical scheme for this case. To understand this scheme let us first look at the situation where one sphere is uniformly reactive [$u_2(\gamma_2) = 1$ and $F_2 = 1$]. Eq. 6 gives

$$k(\infty) = \frac{4\pi DaF_1}{(\kappa a/D)^{-1} + \frac{1}{2}F_1^{-1}\sum_{l=0}^{\infty}\frac{(l + 1/2)[c_1(l)/2\pi]^2}{\mu_l aK_{l+3/2}(\mu_l a)/K_{l+1/2}(\mu_l a) - l}}, \quad (16)$$

where $\mu_l = [(D_1l(l+1))/D]^{1/2}$. Eq. 16 is the same as the results of Solc and Stockmayer (18) and Szabo and coworkers (16, 19). Fig. 2 illustrates the quasichemical scheme for this situation. Translational diffusion (rate constant k_t) brings originally separated proteins 1 and 2^+ ("+" signifies the uniform reactivity of protein 2) together to form a pair 12^+. Depending on whether the reactive part of protein 1 is in contact with protein 2, two kinds of pairs, 1^+2^+ and 1^-2^+, are formed, the former with rate constant F_1k_t and the latter $(1 - F_1)k_t$. They can convert [rate constants k_1 and k_1', $k_1/k_1' = F_1/(1 - F_1)$] by means of rotational diffusion. Only the favorably oriented pairs 1^+2^+ can go on to form the product P (rate constant k_x). The rate constant $k(\infty)$ for forming the product is obtained by assuming that the intermediate species 1^+2^+ and 1^-2^+ are under steady-state conditions. The result is

$$k(\infty) = \frac{k_tf_1}{(k_x/k_t')^{-1} + \Lambda_1}, \quad (17a)$$

where

$$\Lambda_1 = \frac{F_1 + k_t'/(k_1 + k_1')}{1 + k_t'/(k_1 + k_1')}. \quad (17b)$$

Eq. 17a is equivalent to Eq. 16 if one makes the identifications

$$k_t = 4\pi Da, \quad (18a)$$

$$k_x/k_t' = \kappa a/D, \quad (18b)$$

and

$$\Lambda_1 = \frac{1}{2}F_1^{-1}\sum_{l=0}^{\infty}\frac{(l + 1/2)[c_1(l)/2\pi]^2}{\mu_l aK_{l+3/2}(\mu_l a)/K_{l+1/2}(\mu_l a) - l}. \quad (18c)$$

When protein 2 is also nonuniformly reactive, it can be either 2^+ or 2^-, resulting in four intermediate species. The quasichemical scheme gives

$$k(\infty) = \frac{k_tF_1F_2}{(k_x/k_t')^{-1} + \Lambda_1\Lambda_2 + \psi}, \quad (19a)$$

where

$$\psi^{-1} = (1 - \Lambda_1)^{-1}(1 - \Lambda_2)^{-1} + (1 - \Lambda_1)^{-1}(\Lambda_2 - F_2)^{-1} + (1 - \Lambda_2)^{-1}(\Lambda_1 - F_1)^{-1}. \quad (19b)$$

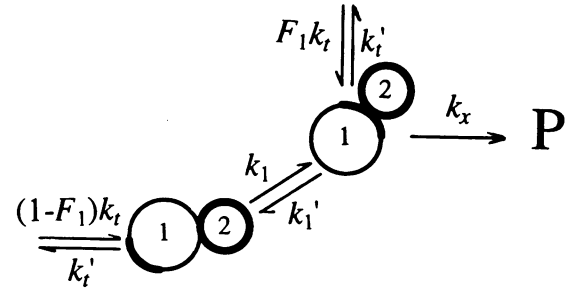

FIGURE 2 The quasichemical scheme when one protein is uniformly reactive.

Solc and Stockmayer (18) suggested combining Eqs. 19 with the identifications of Eqs. 18 (similarly for Λ_2) to find the steady-state rate constant. Berg (21) further simplified this approach of calculating $k(\infty)$ through approximating the sum in Eq. 18c (similarly for Λ_2) by elementary functions. If the reactive patch on the ith protein is the region between $\gamma_i = 0$ and $\gamma_i = \delta_i$, then $c_i(l)/2\pi = [P_{l-1}(\cos\delta_i) - P_{l+1}(\cos\delta_i)]/(2l+1)$. Berg found that Eq. 18c can be approximated by [$\xi_i = \sqrt{(1 + D_i a^2/D)/2}$]:

$$\Lambda_i/F_i = \frac{\xi_i + \cot(\delta_i/2)}{\xi_i + \sin(\delta_i/2)\cos(\delta_i/2)}. \qquad (20)$$

To assess the validity of the quasichemical scheme, in Fig. 3 we compare its steady-state rate-constant, given by Eqs. 19 with Λ_i either from Eq. 18c or from Eq. 20, and $k(\infty)$ of the constant-flux approximation, given by Eq. 6. The special functions involved were evaluated using the codes provided in the book of Press et al. (28). It can be seen that the quasichemical scheme using both forms of Λ_i is satisfactory. Thus, Eqs. 19–20 provide a simple analytical formula for calculating the steady-state rate constant when the interaction potential is zero.

It is interesting to look at the patch size dependence of the rate coefficient in this case when both reactive patches are very small. We see from Eq. 10 that the initial value $k(0)$ is proportional to the fractional reactive surface area $4\pi a^2 F_1 F_2 = 4\pi a^2 \sin^2(\delta_1/2)\sin^2(\delta_2/2)$, thus scales as δ^4, where $\delta_1 \sim \delta_2 \sim \delta$. This is not the behavior of the long-time steady-state rate constant. For small patches Eqs. 19–20 give in the diffusion-controlled limit

$$k_D(\infty)/4\pi Da = F_1\xi_2 \tan(\delta_2/2) + F_2\xi_1 \tan(\delta_1/2). \qquad (21)$$

Consequently $k_D(\infty)$ scales as δ^3. The rate constant is much larger than what would be naively guessed from a geometrical argument.

A potential for which the functions $f_l(r;\mu)$ can be solved explicitly is the one arising from the Coulomb interaction, $\beta U(r) = Q/r$, under the condition $\mu = 0$. This condition is satisfied when one considers the steady-state situation of a uniformly reactive protein diffusing around an immobile nonuniformly reactive protein. The solution can be accomplished by making the variable changes $f_l(r;0) = \exp[\beta U(r)/2]g_l(r)/r$ and $r = |Q|/2x$. The results are

$$f_l(r;0) = e^{Q/2r}\sqrt{\pi/|Q|r}\, I_{l+1/2}(|Q|/2r), \qquad (22)$$

where $(\pi/2x)^{1/2} I_{l+1/2}(x)$ are the modified spherical Bessel functions of the first kind. The steady-state rate constant of a uniformly reactive protein diffusing toward an immobile nonuniformly reactive protein is [$q = Q/2a = \beta U(a)/2$]

$$k(\infty) = \frac{4\pi Da F_1 e^{-Q/a}}{(\kappa a/D)^{-1} + \frac{1}{4}F_1^{-1}\sum_{l=0}^{\infty}\frac{[P_{l-1}(\cos\delta_1) - P_{l+1}(\cos\delta_1)]^2/(2l+1)}{|q|I_{l+3/2}(|q|)/I_{l+1/2}(|q|) + q + l + 1}}. \qquad (23)$$

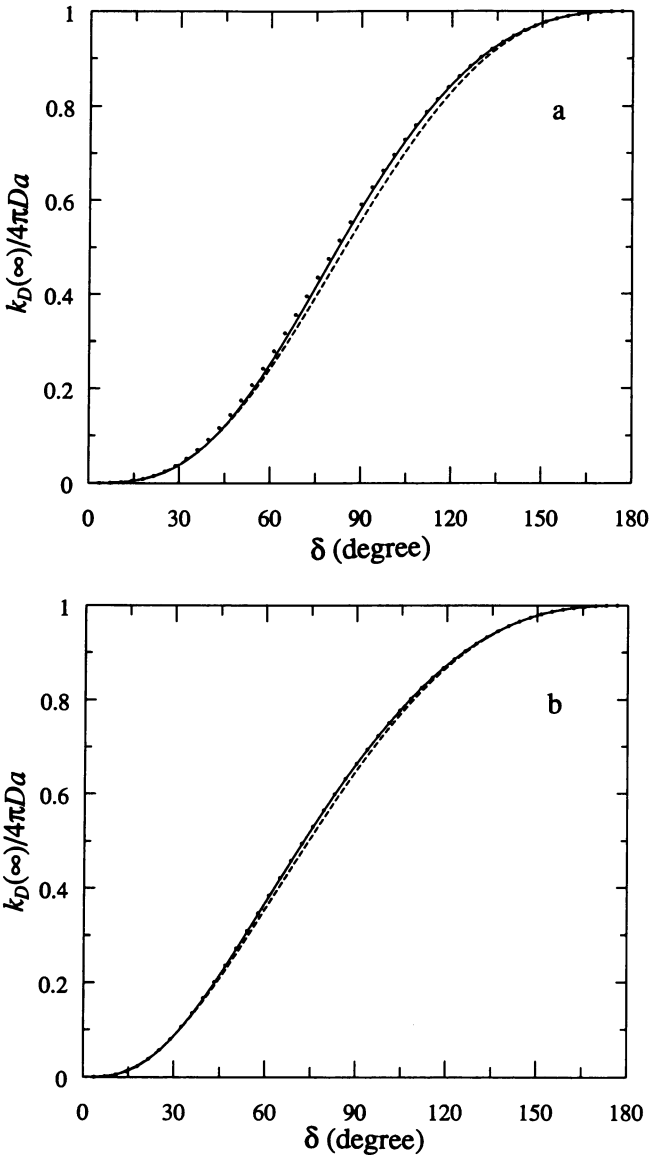

FIGURE 3 Comparison of the steady-state rate constant from the constant-flux approximation (Eq. 6; *solid curve*) with the quasichemical approximation of Solc and Stockmayer (Eqs. 19 and 18c; *dotted curve*) and Berg's further simplification (Eqs. 19 and 20; *dashed curve*). The translational and rotational diffusion coefficients were calculated using the Stokes–Einstein expressions, thus $D_1a^2/D = (3/4)(a_2/a_1)(1 + a_2/a_1)$ and similarly for D_2a^2/D. (*a*) $a_1/a_2 = 1$, (*b*) $a_1/a_2 = 10$. The two spheres have equal patches, $\delta_1 = \delta_2 = \delta$, and the diffusion-controlled limit is considered.

This result in the diffusion-controlled limit ($\kappa \to \infty$) has recently been tested (29). Eq. 23 also provides insight to the effect of the interaction potential when the reactive patch is small ($\delta_1 \ll 1$). In this limit $[P_{l-1}(\cos\delta_1) - P_{l+1}(\cos\delta_1)]^2/(2l+1)$ increases with l and terms with large l have more and more weight in the summation over l. For these terms the potential has less and less effect. Consequently the denominator of Eq. 23 becomes independent of the potential and the rate constant with the potential is simply that without the potential multiplied by the Boltzmann factor $\exp[-\beta U(a)]$. To see this effect clearly we plot in Fig. 4 $\exp[\beta U(a)]k_D(\infty)/4\pi Da$ against the patch size δ_1 at contact potentials of $\beta U(a) = 4, 2, 0, -2, -4$. For small patch sizes all the curves coincide.

The above argument about the effect of the interaction potential when the reactive patches are small is expected to be a general one. Thus, for small patches, we have the following formula for the steady-state rate constant under an arbitrary centrosymmetric interaction potential $U(r)$:

$$e^{\beta U(a)}k(\infty)/4\pi Da = \frac{[F_1\xi_2 \tan(\delta_2/2) + F_2\xi_1 \tan(\delta_1/2)]F_1F_2\kappa a/D}{F_1\xi_2 \tan(\delta_2/2) + F_2\xi_1 \tan(\delta_1/2) + F_1F_2\kappa a/D}. \quad (24)$$

For larger patches the full summation of Eq. 6 will have to be calculated. Reference 29 contains a simple method for numerically finding the functions $f_l[r; \mu_{l_1l_2}(s)]$ under an arbitrary potential.

The reactivity in this section has been represented by a radiation boundary condition, given in Eq. 3. It can be represented in a different but equivalent manner (26).

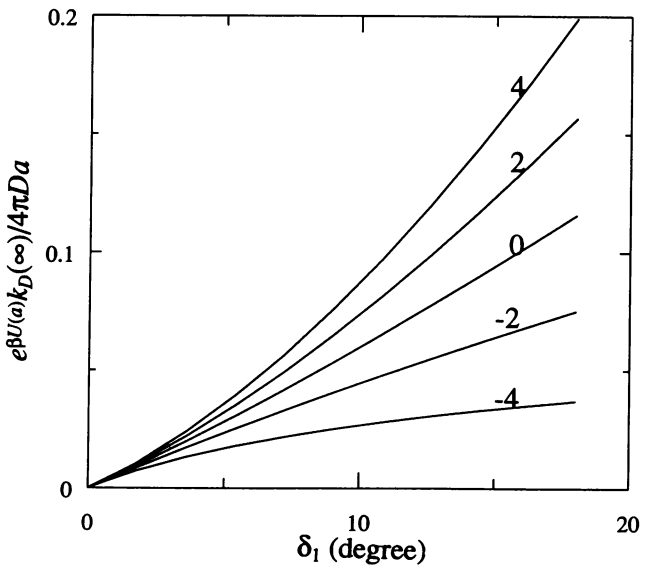

FIGURE 4 The rate constant, scaled by the contact potential, of a uniformly reactive sphere diffusing toward an immobile patched sphere in the Coulombic potential as a function of the patch size. The magnitude of the contact potential, $\beta U(a)$, is shown above the curves.

In this representation the boundary is completely reflecting,

$$De^{-\beta U(r)}\frac{\partial}{\partial r}e^{\beta U(r)}P = 0, \quad r = a. \quad (25)$$

Instead a sink term is added to the translational–rotational diffusion equation,

$$\frac{\partial P}{\partial t} = D\nabla\cdot e^{-\beta U(r)}\nabla e^{\beta U(r)}P + \sum_{i=1}^{2} D_i\Omega_i\cdot\Omega_i P - \kappa u_1(\gamma_1)u_2(\gamma_2)\delta(r-a)P. \quad (26)$$

The equivalence of the two representations can be easily checked by integrating both sides of Eq. 26 over r from a to $a+\epsilon$ and letting $\epsilon \to 0$. If we represent the delta-function by the following step-function,

$$\delta(r-a) = 1/\epsilon, \quad a < r < a+\epsilon; \qquad 0, \quad a > a+\epsilon, \quad (27)$$

the sink term in Eq. 26 has a simple interpretation. When the interprotein distance is in the region $[a, a+\epsilon]$ and the prospective contact point is in both reactive patches, i.e., when a reactive complex is formed, the pair has a lifetime of κ/ϵ. In the general protein–protein diffusional association model to be discussed in the following sections, both the restriction that the interaction potential depends only on the interprotein distance and the restriction that the reactive complex is formed only when the spheres are at contact will be lifted.

INTERACTION POTENTIAL

We now describe the method for obtaining the interaction potential between two spheres bearing point charges and immersed in a salt solution. As the Poisson equation governing the interiors of the spheres is linear and we will restrict to the linearized Poisson–Boltzmann equation governing the outside of the spheres S_1 and S_2, the electrostatic potential at any point is the sum of the contributions of all the charges. So first we will deal with a single point charge q inside the first sphere (see Fig. 5). We will first derive from Green's theorem some integral equations satisfied by the electrostatic potential V and solve them under a particular basis set. The contributions from all the charges are then summed and the free energy of the system is obtained from the electrostatic potential. The interaction potential U between the two spheres is just the free energy of the system relative to a particular standard state.

From Green's theorem it is simple to show that the electrostatic potential $V_i = V(\mathbf{r}_i)$ inside the surface S_i, $i = 1$ or 2, satisfies the integral equation (30)

$$4\pi V_i = \frac{4\pi q(2-i)}{\epsilon_{in}|\mathbf{r}_i - \mathbf{r}_q|} + \int_{S_i} dS\left(\frac{1}{\epsilon_{in}|\mathbf{r}_i - \mathbf{r}_{si}|}g_i - f_i\mathbf{n}_i\cdot\nabla_{si}\frac{1}{|\mathbf{r}_i - \mathbf{r}_{si}|}\right), \quad (28a)$$

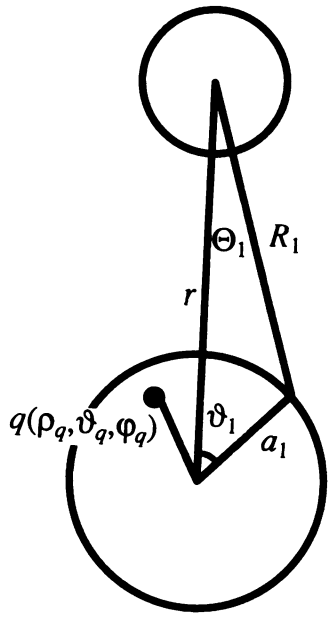

FIGURE 5 The geometry of two charge-bearing spheres used in calculating their free energy.

$$f_i = V(\mathbf{r}_{si}), \quad g_i = \epsilon_{in}\mathbf{n}_i \cdot \nabla_{si} V(\mathbf{r}_{si}), \tag{28b, c}$$

where $\mathbf{n}_i$ is the unit vector along the normal of the surface S_i, and ϵ_{in} is the interior dielectric constant. The factor $2 - i$ is designed to give 1 for the first sphere and 0 for the second sphere. When the position $\mathbf{r}_i$ is moved onto the surface S_i, $\mathbf{r}_i = \mathbf{r}'_{si}$, we have the following self-consistent relation for f_i:

$$2\pi f'_i = \frac{4\pi q(2-i)}{\epsilon_{in}|\mathbf{r}'_{si} - \mathbf{r}_q|} + \int_{S_i} dS\left(\frac{1}{\epsilon_{in}|\mathbf{r}'_{si} - \mathbf{r}_{si}|} g_i - f_i \mathbf{n}_i \cdot \nabla_{si} \frac{1}{|\mathbf{r}'_{si} - \mathbf{r}_{si}|}\right). \tag{29}$$

Similarly, the electrostatic potential $V_o = V(\mathbf{r}_o)$ outside of $S_1 + S_2$ satisfies the integral equation

$$-4\pi V_o = \sum_{i=1}^{2} \int_{S_i} dS\left(\frac{e^{-|\mathbf{r}_o - \mathbf{r}_{si}|/\lambda}}{\epsilon_{ou}|\mathbf{r}_o - \mathbf{r}_{si}|} g_i - f_i \mathbf{n}_i \cdot \nabla_{si} \frac{e^{-|\mathbf{r}_o - \mathbf{r}_{si}|/\lambda}}{|\mathbf{r}_o - \mathbf{r}_{si}|}\right), \tag{30}$$

where ϵ_{ou} is the outside dielectric constant and λ is the Debye–Huckel screening length. The boundary conditions for the electrostatic potential have been built into Eq. 30. When the position $\mathbf{r}_o$ is moved onto the surfaces S_j, $\mathbf{r}_o = \mathbf{r}'_{sj}$, we have two other self-consistent relations for f_i and g_i:

$$-2\pi f'_j = \sum_{i=1}^{2} \int_{S_i} dS\left(\frac{e^{-|\mathbf{r}'_{sj} - \mathbf{r}_{si}|/\lambda}}{\epsilon_{ou}|\mathbf{r}'_{sj} - \mathbf{r}_{si}|} g_i - f_i \mathbf{n}_i \cdot \nabla_{si} \frac{e^{-|\mathbf{r}'_{sj} - \mathbf{r}_{si}|/\lambda}}{|\mathbf{r}'_{sj} - \mathbf{r}_{si}|}\right). \tag{31}$$

A development similar to Eqs. 30 and 31 has appeared in the context of colloidal particles (31). Eqs. 29 and 31 determine the surface potentials f_i and their normal derivatives g_i. Once they are determined, Eqs. 28a can be used to determine the potential in the interiors and Eq. 30 can be used to determine the potential in the outside.

To solve for f_i and g_i, we expand them in terms of spherical harmonics

$$f_i = \sum_{l,m} f_{ilm} Y_{lm}(\vartheta_i, \varphi_i), \tag{32}$$

and similarly for g_i, where (ϑ_i, φ_i) express $\mathbf{n}_i$ in spherical coordinates. When they are inserted into Eqs. 29 and 31, one obtains an infinite set of linear equations for the expansion coefficients,

$$f_{ilm} - \sum_{l'} A_{ill'm} f_{i'l'm} = B_{ilm}, \tag{33}$$

where $i' = 2$ when $i = 1$ and $i' = 1$ when $i = 2$. The constants are

$$A_{ill'm} = \frac{C_{ill'm}\sqrt{x_{i'}}[(1 - \epsilon_{in}/\epsilon_{ou})l' I_{l'+1/2}(x_{i'}) + x_{i'} I_{l'+3/2}(x_{i'})]}{I_{l+1/2}(x_i)[(1 + l + l\epsilon_{in}/\epsilon_{ou})K_{l+1/2}(x_i) + x_i K_{l-1/2}(x_i)]}, \tag{34a}$$

$$B_{1lm} = \frac{K_{l+1/2}(x_1)h_{lm}}{(1 + l + l\epsilon_{in}/\epsilon_{ou})K_{l+1/2}(x_1) + x_1 K_{l-1/2}(x_1)}, \tag{34b}$$

$$B_{2lm} = \frac{\sum_{l'} C_{2ll'm}\sqrt{x_1} I_{l'+1/2}(x_1) h_{l'm}}{I_{l+1/2}(x_2)[(1 + l + l\epsilon_{in}/\epsilon_{ou})K_{l+1/2}(x_2) + x_2 K_{l-1/2}(x_2)]}. \tag{34c}$$

We have defined $x_i = a_i/\lambda$,

$$h_{lm} = \frac{4\pi q}{\epsilon_{ou} a_1} (\rho_q/a_1)^l Y^*_{lm}(\vartheta_q, \varphi_q), \tag{35a}$$

and

$$C_{ill'm} = \int \sin\vartheta_i \, d\vartheta_i \, d\varphi_i Y^*_{lm}(\vartheta_i, \varphi_i) Y_{lm}(\Theta_i, \varphi_i) \times K_{l'+1/2}(R_i/\lambda)/\sqrt{R_i/\lambda}, \tag{35b}$$

where $(\rho_q, \vartheta_q, \varphi_q)$ is the position of charge q in spherical coordinates, $R_i = \sqrt{r^2 + a_i^2 - 2ra_i \cos\vartheta_i}$, and $\cos\Theta_i = (r - a_i \cos\vartheta_i)/R_i$. Note that B_{1lm} are the solutions that Kirkwood (10) found for a single charge-bearing sphere, as should be the case when the second sphere is absent. When both spheres are present there are no analytical solutions anymore. We obtained f_{ilm} by truncating Eqs. 33 at appropriate orders and inverting the matrix involved by LU decomposition (28). The coefficients

$C_{ill'm}$ in general could not be found in closed form and were evaluated numerically. Some particular elements, however, can be found analytically, e.g.,

$$C_{i00} = \sqrt{(2l+1)\pi/2}\, I_{l+1/2}(x_i) K_{l+1/2}(r/\lambda)/\sqrt{x_i r/\lambda}. \quad (36)$$

They serve as checks of the numerical evaluations.

In terms of f_{ilm}, the potentials inside the spheres are

$$V(\mathbf{r}_i; q) = \frac{q(2-i)}{\epsilon_{in}|\mathbf{r}_i - \mathbf{r}_q|} - \frac{q(2-i)a_1/\rho_q}{\epsilon_{in}|\mathbf{r}_i - (a_1/\rho_q)^2\mathbf{r}_q|} + \psi(\mathbf{r}_i; q), \quad (37a)$$

$$\psi(\mathbf{r}_i; q) = \sum_{l,m} (\rho_i/a_i)^l f_{ilm} Y_{lm}(\vartheta_i, \varphi_i), \quad (37b)$$

where $(\rho_i, \vartheta_i, \varphi_i)$ are the positions of $\mathbf{r}_i$ in spherical coordinates.

Suppose that there are N_i charges inside the ith sphere, then aside from a constant, the total electrostatic potential at position $\mathbf{r}_i$ is

$$\psi(\mathbf{r}_i) = \sum_{i=1}^{2} \sum_{n_i=1}^{N_i} \psi(\mathbf{r}_i; q_{n_i}). \quad (38)$$

The free energy of the system is (10)

$$W = \frac{1}{2} \sum_{i=1}^{2} \sum_{n_i=1}^{N_i} q_{n_i} \psi(\mathbf{r}_{n_i}). \quad (39)$$

The interaction potential U is the free energy of the system relative to the state that the two spheres are at infinite separation. In that state the free energy of the system is the sum of the free energies W_i of the two spheres; each is the problem solved analytically by Kirkwood (reference 10; also see Eqs. 34b). Thus

$$U = W - W_1 - W_2. \quad (40)$$

ASSOCIATION RATE: THE CASE OF CYTOCHROME c AND CYTOCHROME c PEROXIDASE

In this section we continue the development of our protein–protein diffusional association model by letting the proteins diffuse and react in the potential field calculated in the last section. In the model there is some particular subspace Γ in the configuration space of the system where the system, termed reaction complex, can disappear by conversion to the product, unless it is rescued by diffusing out. Of course diffusion also plays the reverse role by moving the system into that region.

The time-dependent rate coefficient $k(t)$ of this model is then found through Brownian dynamics simulations by using the algorithm developed earlier by us (15). Originally this algorithm dealt only with the case of a uniformly reactive protein diffusing toward an immobile nonuniformly reactive protein. According to this algorithm, Brownian dynamics trajectories of the uniformly reactive protein are launched from the reaction region Γ and propagated. Every time it gets into the reaction region it has a certain lifetime τ. If it stays longer than τ, its trajectory is terminated. All the trajectories have a cutoff time interval T_{cut} to be propagated. When all the trajectories are finished, the survival fraction of all the trajectory at any time $t < T_{cut}$ gives $k(t)/k(0)$, and $k(0)$ can be found analytically.

Extension of this algorithm to deal with the general protein–protein diffusional association model is straightforward. The only complication is that, in addition to the translational Brownian motion of the interprotein displacement vector, the rotational Brownian motion of the two proteins has to be included. This completes the description of our protein–protein diffusional association model and the calculation of its time-dependent rate coefficient through Brownian dynamic simulations.

We now apply this method to the diffusional association of a model system of cytochrome c and cytochrome c peroxidase introduced by Northrup et al. (22). In this system the proteins were axisymmetric spheres with three charges on their symmetry axes and 10° reactive patches around them. The radii of cytochrome c and cytochrome c peroxidase were 14 and 21 Å, respectively. These and other relevant parameters of the system are listed in Table 1. We make one change from the model of Northrup et al. They put the noncentral charges 1.0 Å beneath the protein surfaces. These charges are shifted further to the protein centers to moderate somewhat the effects of the surface charges, now 9.3 and 6.2 Å, respectively, beneath the surfaces of cytochrome c and cytochrome c peroxidase.

TABLE 1 Parameters of the charge-bearing sphere model of the cytochrome c and cytochrome c peroxidase system

Parameters	Cytochrome c peroxidase	Cytochrome c
Protein radii a_i, Å	21	14
Translational diffusion constant D*	2.58×10^{-2} Å/ps	
Rotational diffusion constants D_i*, ps^{-1}	1.76×10^{-5}	5.9×10^{-5}
Central charges, e	−12	+8
Surface charges, e‡	∓2.21	±2.29
Depth of surface charges, Å	9.3	6.2
Reaction region thickness ϵ	0.35 Å	
Reactive patch sizes δ_i, deg	10	10
Lifetime of reaction complex τ	47.5 ps	

* All the diffusion constants were calculated using the Stokes–Einstein expressions with the temperature at 25°C and a viscosity of 1.0 cP.
‡ The surface charges of each protein are located on the symmetry axis of the protein, on opposite sides of the center, and have equal distance to the center. The first sign refers to the charge at the front of the reactive patch, the second sign refers to the charge at the back.

Northrup et al. (22) treated the electrostatics of the system by the Coulomb-type charge–charge interactions, each modified by a Debye–Huckel screening. With the method of the last section we can treat the electrostatics of this system realistically, taking into account the low dielectric constant of both protein interiors and the screening of the salt. For the protein interiors we choose a dielectric constant $\epsilon_{in} = 4.0$; for the solvent we choose $\epsilon_{ou} = 78.5$. Fig. 6 shows a plot of the interaction potential as a function of the interprotein distance when the protein axes are lined with the interprotein displacement vector at ionic strength $I = 0.16$ m, corresponding to a Debye screening length $\lambda = 3.04 I^{-1/2} = 7.6$ Å. The contact potential is $-3.9 k_B T$, about -2.3 kcal/mol at room temperature.

Besides the treatment of the electrostatic interaction, our method for studying the diffusional association of this model system of cytochrome *c* and cytochrome *c* peroxidase has a difference in the reaction criterion. While Northrup et al. (22) used an absorbing boundary condition ($\kappa \to \infty$ limit of the radiation boundary condition) in treating the reaction, as described in the beginning of this section we use a finite region in which the reaction complex has a finite lifetime τ. This method is more general in the sense that by making the reaction region thinner and thinner as to collapse to the boundary $r = a$ and reducing the lifetime τ accordingly, we get the radiation and the absorbing boundary conditions. It can deal with precisely the bond-formation criterion of protein–protein association recently proposed by Northup and Erickson (32). Specifically, we choose the following reaction region

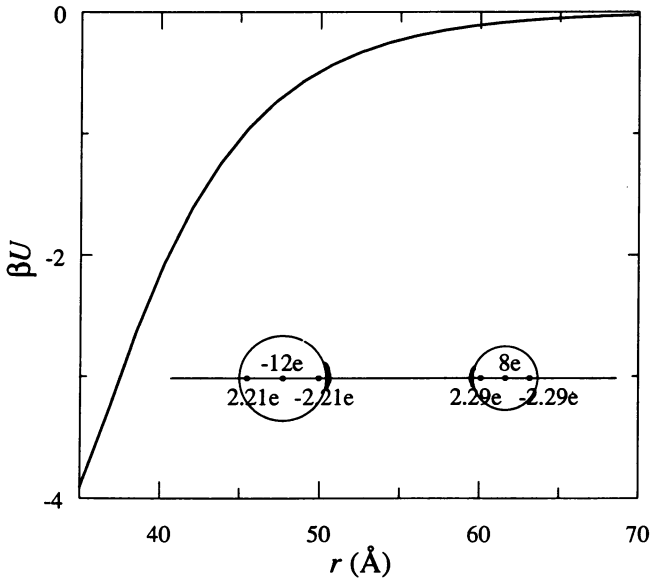

FIGURE 6 The interaction potential in the model system of cytochrome *c* and cytochrome *c* peroxidase as a function of the interprotein separation when the proteins have their axes lined along the displacement vector (as shown in the *inset*). The ionic strength is $I = 0.16$ m.

$$\Gamma: \quad r \in (a, a + \epsilon), \quad \gamma_i \in (0, \delta_i). \tag{41}$$

The thickness ϵ of the region is assigned to be $10^{-2}a = 0.35$ Å, and the sizes δ_i of both patches are assigned to be 10°. As for the lifetime of the reaction complex, it is chosen to be $\tau = 47.5$ ps. This would give $\kappa a = \epsilon a/\tau$ 10 times the diffusion constant D. This choice of the reaction region, combined with the above choice of the sites of the surface charges, gives roughly the same diffusional association rate constant as found in experiments (23) at the ionic strength $I = 0.16$ m (see below).

The diffusion–reaction equation of the model system now can be written down. This system differs from the one described by Eq. 26 in two respects. First, the interaction potential U now depends not only on the magnitude r of the interprotein displacement but also on its orientation $\mathbf{e}$ and the orientations $\mathbf{e}_1$ and $\mathbf{e}_2$ of the spheres as well. Second, the reaction region Γ now has a finite thickness. Taking both factors into account, we obtain

$$\frac{\partial P}{\partial t} = D\nabla \cdot e^{-\beta U} \nabla e^{\beta U} P + \sum_{i=1}^{2} D_i \Omega_i \cdot e^{-\beta U} \Omega_i e^{\beta U} P - \tau^{-1} u_\Gamma P, \tag{42}$$

where u_Γ is a step-function that is 1 when the system is in the reaction region Γ and 0 otherwise. If we use $\mathbf{x}$ to denote the configuration $(\mathbf{r}, \mathbf{e}_1, \mathbf{e}_2)$ and $d\mathbf{x} = d\mathbf{r} d\mathbf{e}_1 d\mathbf{e}_2$ to denote its volume element, the time-dependent rate coefficient of this system is (24)

$$k(t) = \tau^{-1} \int_{\mathbf{x} \in \Gamma} d\mathbf{x} P(\mathbf{x}, t). \tag{43}$$

Its initial value is readily obtained, as at $t = 0$, P starts from the equilibrium distribution $P_{eq}(\mathbf{x}) = (4\pi)^{-2} \times \exp[-\beta U(\mathbf{x})]$ (see Appendix A); thus,

$$k(0) = \tau^{-1} \int_{\mathbf{x} \in \Gamma} d\mathbf{x} P_{eq}(\mathbf{x}) = \tau^{-1} \int_{\mathbf{x} \in \Gamma} d\mathbf{x} (4\pi)^{-2} e^{-\beta U(\mathbf{x})}. \tag{44}$$

However, the whole time dependence of $k(t)$ is not so simple. It can be found by expressing $k(t)$ in terms of survival probabilities, which are obtainable through Brownian dynamics simulations. Reference 15 contains the details of this procedure when one protein is immobile and the other is uniformly reactive. Here we do this for the more general situation.

The procedure evolves around the Green function $G(\mathbf{x}, t | \mathbf{x}_0, 0)$ of Eq. 42. It satisfies the initial condition

$$G(\mathbf{x}, 0 | \mathbf{x}_0, 0) = \delta(\mathbf{x} - \mathbf{x}_0) \tag{45}$$

and the detailed balance condition (33)

$$G(\mathbf{x}, t | \mathbf{x}_0, 0) P_{eq}(\mathbf{x}_0) = G(\mathbf{x}_0, t | \mathbf{x}, 0) P_{eq}(\mathbf{x}). \tag{46}$$

The distribution function $P(\mathbf{x}, t)$ is obtained from the Green function through

$$P(\mathbf{x}, t) = \int d\mathbf{x}_0 G(\mathbf{x}, t|\mathbf{x}_0, 0) P_{eq}(\mathbf{x}_0). \quad (47)$$

The survival probability $S(t|\mathbf{x}_0)$ of the system starting from the configuration $\mathbf{x}_0$ is just the integration of $G(\mathbf{x}, t|\mathbf{x}_0, 0)$ over the configuration space,

$$S(t|\mathbf{x}_0) = \int d\mathbf{x} G(\mathbf{x}, t|\mathbf{x}_0, 0). \quad (48)$$

Comparing Eqs. 46–48, one finds

$$P(\mathbf{x}_0, t) = S(t|\mathbf{x}_0) P_{eq}(\mathbf{x}_0). \quad (49)$$

Consequently we can express $k(t)$ in terms of survival probabilities,

$$k(t)/k(0) = \int_{\mathbf{x}_0 \in \Gamma} d\mathbf{x}_0 S(t|\mathbf{x}_0) p(\mathbf{x}_0), \quad (50a)$$

where the normalized distribution $p(\mathbf{x}_0)$ is

$$p(\mathbf{x}_0) = P_{eq}(\mathbf{x}_0) \Big/ \int_{\mathbf{x}_0 \in \Gamma} d\mathbf{x}_0 P_{eq}(\mathbf{x}_0)$$
$$= e^{-\beta U(\mathbf{x}_0)} \Big/ \int_{\mathbf{x}_0 \in \Gamma} d\mathbf{x}_0 e^{-\beta U(\mathbf{x}_0)}. \quad (50b)$$

Eq. 50a has a simple interpretation. If one starts trajectories from the distribution $p(\mathbf{x}_0)$ and propagates them, the survival fraction at any time t gives $k(t)/k(0)$.

We now deal with the propagation of the Brownian dynamics trajectories. Appendix B derives algorithms for picking configurations from the short-time Green function $G_0(\mathbf{x}, \Delta t|\mathbf{x}_0, 0)$ in the absence of reaction (i.e., $\tau \to \infty$). They are

$$\mathbf{r} = \mathbf{r}_0 - (\beta \nabla U) D \Delta t + \mathbf{C}\sqrt{2D\Delta t}, \quad (51a)$$

$$\mathbf{e}_i = \mathbf{e}_{i0} - \left[2\mathbf{e}_{i0} + \beta \frac{\partial U}{\partial \mathbf{e}_{i0}} - \left(\mathbf{e}_{i0} \cdot \beta \frac{\partial U}{\partial \mathbf{e}_{i0}}\right)\mathbf{e}_{i0}\right] D_i \Delta t + (\mathbf{1} - \mathbf{e}_{i0}\mathbf{e}_{i0}) \mathbf{C}_i \sqrt{2 D_i \Delta t}, \quad (51b)$$

where $\mathbf{1}$ is the unit matrix and $\mathbf{C}$ and $\mathbf{C}_i$ are vectors of Gaussian random numbers with the following properties

$$\langle \mathbf{C} \rangle = 0, \quad (52a)$$

$$\langle \mathbf{C}\mathbf{C}^{\mathrm{T}} \rangle = \mathbf{1}. \quad (52b)$$

At short times the Green functions in the presence and absence of reaction are related by (34)

$$G(\mathbf{x}, \Delta t|\mathbf{x}_0, 0) = e^{-\Delta t[u_\Gamma(\mathbf{x}) + u_\Gamma(\mathbf{x}_0)]/2\tau} G_0(\mathbf{x}, \Delta t|\mathbf{x}_0, 0). \quad (53)$$

Thus reaction is taken into account by terminating a fraction $1 - \exp\{-\Delta t[u_\Gamma(\mathbf{x}) + u_\Gamma(\mathbf{x}_0)]/2\tau\}$ of the nonreacting trajectories at each step. Specifically, at each step a new configuration $\mathbf{x} = (\mathbf{r}, \mathbf{e}_1, \mathbf{e}_2)$ is generated using Eqs. 51. Then a random number $\mathcal{R}$ uniformly distributed between 0 and 1 is generated. The new configuration is accepted and the trajectory is propagated forward if $\mathcal{R} < \exp\{-\Delta t[u_\Gamma(\mathbf{x}) + u_\Gamma(\mathbf{x}_0)]/2\tau\}$; otherwise the trajectory is terminated.

The derivatives $\partial U/\partial \mathbf{x}$ in Eqs. 51 have components along $\mathbf{x} = (\mathbf{r}, \mathbf{e}_1, \mathbf{e}_2)$ involving $\partial U/\partial R$, $\partial U/\partial \cos\gamma_i$, and $\partial U/\partial \phi_{12}$, $\phi_{12} = \phi_2 - \phi_1$. We broke r between a and $2a$ into 10 segments, $\cos\gamma_i$ between -1 and 1 into 20 pieces, and ϕ_{12} between 0 and 2π into 20 pieces. This results in 8×10^4 cells. At the center of each cell, we calculated $\partial U/\partial R$, $\partial U/\partial \cos\gamma_i$, and $\partial U/\partial \phi_{12}$ using central differences. Subsequently, the components of $\partial U/\partial \mathbf{x}$ along $\mathbf{x} = (\mathbf{r}, \mathbf{e}_1, \mathbf{e}_2)$ were stored as a table. Tabulating the derivatives $\partial U/\partial \mathbf{x}$ in the 8×10^4 cells took $\sim$10 h on a Convex C240 computer. In the course of the Brownian dynamics simulations, the cell corresponding to the configuration at each step was located and the components of $\partial U/\partial \mathbf{x}$ at the cell center were looked up. When multiplied by the unit vectors $\mathbf{e}$ and $\mathbf{e}_i$, they gave the derivatives $\partial U/\partial \mathbf{x}$ at that step. The derivatives beyond $r = 2a$ were assumed to be 0. This does not pose a severe approximation for two reasons. First, because of the salt screening the interaction potential at an interprotein separation of $r = 2a$ is reduced dramatically (see Fig. 6). Furthermore, within the cutoff time interval T_{cut} the trajectories, started near $r = a$, rarely venture as far as $r = 2a$.

To find the time-dependent rate coefficient of the cytochrome c and cytochrome c peroxidase model system, we started $J = 4000$ configurations with r at a, $\cos\gamma_i$ uniformly distributed between $\cos\delta_i$ and 1, and ϕ_{12} uniformly distributed between 0 and 2π. The average Boltzmann factor

$$\langle e^{-\beta U(\mathbf{x}_0)} \rangle_a = \int_{\mathbf{x}_0 \in \Gamma} d\mathbf{x}_0 e^{-\beta U(\mathbf{x}_0)} \delta(r_0 - a) \Big/ \int_{\mathbf{x}_0 \in \Gamma} d\mathbf{x}_0 \delta(r_0 - a) \quad (54)$$

of these configurations is 145.9, 46.4, and 18.8, respectively, at ionic strengths of $I = 0.1$, 0.16, and 0.25 m. Another 4000 configurations were started at $r = a + \epsilon$. Their average Boltzmann factor $\langle e^{-\beta U(\mathbf{x}_0)} \rangle_{a+\epsilon}$ is 129.9, 41.9, and 17.2, respectively, for these ionic strengths. These configurations were then propagated using the following time steps:

$$\Delta t = 2.37 \times 10^{-2} \text{ ps}, \quad a < r < a + \epsilon;$$
$$2.37 \times 10^{-2} \text{ ps} + [(r - \epsilon)/a - 1]^2 \times 23.7 \text{ ps}, \quad r > a + \epsilon.$$

For comparison, trajectories when the interaction potential was turned off (i.e., $I \to \infty$) were also generated using the above protocol, with the exception that the coefficient of the distance-dependent part of the step size increased from 23.7 to 237 ps. The boundary $r = a$ was reflecting and was treated in the following manner.

Whenever a configuration led to collision, i.e., $r < a$, that configuration was accepted as the new one and propagation was started from there again.

All trajectories were terminated either when they were stopped due to reaction or when they reached a cutoff time interval $T_{cut} = 1187$ ps. 4000 trajectories in the presence of the interaction potential took ~4 h on a Convex C240 computer. In the absence of the interaction potential they took ~20 min. The weighted survival fractions of these trajectories are

$$S_b(t) = \frac{1}{J}\sum_{j=1}^{J} u(t_j - t)e^{-\beta U(\mathbf{x}_{0j})}/\langle e^{-\beta U(\mathbf{x}_0)}\rangle_b, \qquad b = a \quad \text{or} \quad a + \epsilon, \quad (55)$$

where $\mathbf{x}_{0j}$ and t_j are, respectively, the initial configuration and the lifetime of the jth trajectory, and $u(t_j - t)$ is a step function that is 1 when $0 < t < t_j$ and 0 otherwise. Comparing Eqs. 50 and 55, one finds that the time-dependent rate coefficient of the cytochrome c and cytochrome c peroxidase model system is

$$k(t)/k(0) = \frac{\langle e^{-\beta U(\mathbf{x}_0)}\rangle_a S_a(t) + (1 + \epsilon/a)^2\langle e^{-\beta U(\mathbf{x}_0)}\rangle_{a+\epsilon} S_{a+\epsilon}(t)}{\langle e^{-\beta U(\mathbf{x}_0)}\rangle_a + (1 + \epsilon/a)^2\langle e^{-\beta U(\mathbf{x}_0)}\rangle_{a+\epsilon}}. \quad (56)$$

Its initial value is

$$k(0) = 4\pi\kappa a^2 \sin^2(\delta_1/2)\sin^2(\delta_2/2) \times [\langle e^{-\beta U(\mathbf{x}_0)}\rangle_a + (1 + \epsilon/a)^2\langle e^{-\beta U(\mathbf{x}_0)}\rangle_{a+\epsilon}]/2, \quad (57)$$

where $\kappa = \epsilon/\tau$. The initial rate coefficient is 5.6×10^8, 1.8×10^8, 7.3×10^7, and 4.0×10^6 $M^{-1}s^{-1}$, respectively, at ionic strengths of 0.1, 0.16, and 0.25 m and infinity.

The time-dependent rate coefficient scaled by its initial value at these ionic strengths is plotted in Fig. 7. Also plotted in this figure is the radiation boundary limit (i.e., $\epsilon \to 0$ but $\kappa = \epsilon/\tau$ constant) of $k(t)/k(0)$ in the absence of the interaction potential. This was obtained by Laplace inverting Eq. 6 using the algorithm of Stehfest (35). The slight difference between $k(t)/k(0)$ under $\epsilon = 10^{-2}a$ and the radiation boundary limit shows the effect of the thickness of the reaction region. One striking feature of this plot is that even though $k(0)$ changes by two orders of magnitudes due to the change of the Boltzmann factor during this range of ionic strengths, $k(t)/k(0)$ changes very little in the entire time interval simulated. This is reminiscent of what was found previously for a centrosymmetric potential. When the reactive patches that lead to the reaction complex are small, the effect of the interaction potential is simply to scale the association rate coefficient by the Boltzmann factor averaged over the configurations of the reactive complex.

To find the steady-state rate constant $k(\infty)$, we fit the long-time tail of $k(t)/k(0)$ to a function of the form (see reference 15 and Eq. 14)

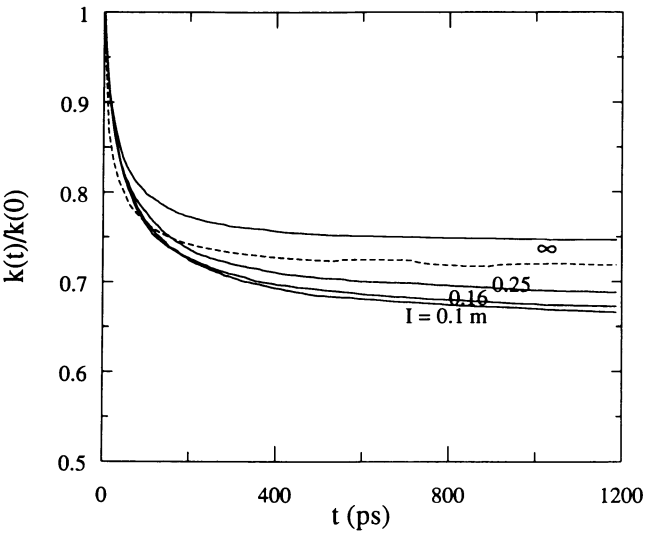

FIGURE 7 The time-dependent rate coefficient, scaled by its initial value, at four ionic strengths. The dashed curve shows the rate coefficient in the radiation boundary limit when the ionic strength is infinite.

$$k(t)/k(0) = \alpha_1 + \alpha_2(a^2/Dt)^{-1/2}. \quad (58)$$

The intercept α_1 of this fit gives $k(\infty)/k(0)$. The results are, at ionic strengths of 0.1, 0.16, and 0.25 m and infinity, $k(\infty)/k(0) = 0.63$, 0.64, 0.66, and 0.73, respectively. The last number in the radiation boundary limit is 0.71 according to Eq. 6. Consequently, the steady-state rate constants at the three finite ionic strengths are 3.5×10^8, 1.2×10^8, and 4.8×10^7 $M^{-1}s^{-1}$. They are compared with the experimental results of Kang et al. (23) in Fig. 8. Our calculations are closer to the experimental results than the studies of Northrup et al. using either the charge-embedded sphere model (22) or their more sophisticated model (8). The experimental ionic strength dependence of the steady-state rate constant is essentially reproduced. Compared with the rate constant 2.9×10^6 $M^{-1}s^{-1}$ in the absence of the potential, the electrostatic interaction between cytochrome c and cytochrome c peroxidase enhances the rate by one to two orders of magnitude at these ionic strengths.

DISCUSSION

We have presented a unified model for protein–protein association processes that are under the influences of electrostatic interaction and diffusion. The proteins are modeled as spheres that bear point charges and undergo translational and rotational Brownian motion. Before association can occur the two spheres have to be aligned properly to form a reaction complex via diffusion. The reaction complex can either go on to form the product or it can dissociate into the separate reactants through diffusion. The electrostatic interaction, like diffusion, influences every step except the one that brings the reaction

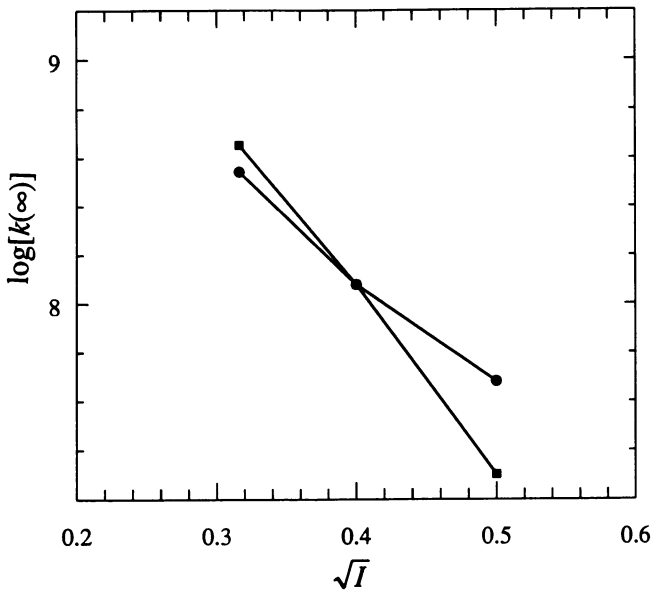

FIGURE 8 Comparison of the simulated (*circles*) and experimental (*squares*) ionic strength dependence of the diffusional association rate constant between cytochrome *c* and cytochrome *c* peroxidase.

complex into the product. The interaction potential is obtained by extending the Kirkwood–Tanford protein model to two charge-embedded spheres and solving the consequent equations under a particular basis set. The time-dependent association rate coefficient is then obtained through Brownian dynamics simulations. This modeling method is applied to the cytochrome *c* and cytochrome *c* peroxidase association process and the results reproduce the experimental dependence of the association rate constant on the solution ionic strength.

Through both simulations of the cytochrome *c* and cytochrome *c* peroxidase system and analytical derivations in the case that the interaction potential is centrosymmetric, we obtain the following remarkable result. When the reactive patches that lead to the reaction complex are small, the effect of the interaction potential is simply to scale the association rate constant by the Boltzmann factor averaged over the configuration space Γ of the reaction complex, $\langle e^{-\beta U} \rangle_\Gamma$. This result allows ready estimate of the association rate constant when a different potential field is present. In particular, we can use it to assess the effect of charge mutations in the proteins. Kang et al. (23) and recently Corin et al. (36) used enzymatic assays to study this effect in the cytochrome *c* and cytochrome *c* peroxidase association process. In the experiments of Corin et al. aspartic acid residues at three locations of cytochrome *c* peroxidase were independently mutated into lysines. To model these mutations we increased the two surface charges in the cytochrome *c* peroxidase sphere model at the front and the back of the reactive patch by two proton charges. For the front charge mutation the average Boltzmann factor decreases from 44.6 to 4.84 at $I = 0.16$ m. This would result in a factor of 9.2 decrease in the association rate constant. On the other hand, for the back charge mutation the average Boltzmann factor changes to 40.2, virtually the same as for the native system. This explains why mutations in the interface of the reaction complex have strong influences on the association rate constant, whereas those away from the interface have minimal effects, as found experimentally by Kang et al. (23) and by Corin et al. (36). It comes about because the former mutations change the interaction potential of the reaction complex significantly and the latter ones do not.

After introducing the charge-embedded sphere model for the cytochrome *c* and cytochrome *c* peroxidase system, Northrup et al. (8) considered a much more sophisticated model. In this model the electrostatic potential around the irregularly shaped cytochrome *c* peroxidase was calculated, taking into account solvent ionic screening. However, cytochrome *c* was treated as a collection of test charges. In reality it is a low dielectric region that excludes ions. To see the effect of this approximation, let us compare the interaction potential in the charge-embedded sphere model when treating cytochrome *c* either as a charge-bearing sphere with low dielectric constant or simply as three test charges. For example, the interaction energy between sphere 1 bearing charge q in Fig. 5 and a test charge q_t on the e axis and a distance r away is

$$U = \frac{q_t q}{\epsilon_{ou} a_1} \sum_{l=0}^{\infty} \frac{K_{l+1/2}(r/\lambda)}{\sqrt{r/\lambda x_1}} \times \frac{(2l+1)(\rho_q/a_1)^l P_l(\cos\vartheta_q)}{(1 + l + l\epsilon_{in}/\epsilon_{ou})K_{l+1/2}(x_1) + x_1 K_{l-1/2}(x_1)}. \quad (59)$$

This is a result of Kirkwood (10) and can be obtained from the equations of the section on interaction potential by making the test charge as a charge-embedded sphere with radius approaching zero. In Fig. 9 we compare the interaction energy using this treatment of cytochrome *c* with that of Fig. 6, where cytochrome *c* is treated realistically. Significant deviation is seen. In this context, we note that the mere presence of sphere 1 modifies the self energy of the test charge. The contribution to the interaction energy due to this modification is

$$U_{sm} = \frac{q_t^2}{2\epsilon_{ou} r} \times \sum_{l=0}^{\infty} \frac{(2l+1)[K_{l+1/2}(r/\lambda)]^2 \times [(1 - \epsilon_{in}/\epsilon_{ou})lI_{l+1/2}(x_1) + x_1 I_{l+3/2}(x_1)]}{(1 + l + l\epsilon_{in}/\epsilon_{ou})K_{l+1/2}(x_1) + x_1 K_{l-1/2}(x_1)}. \quad (60)$$

For example, for an ion that bears unit charge e and has a radius of 1.5 Å in contact with a protein that has a radius of 30 Å, this contribution is $0.62 k_B T$ at $I = 0.16$ m. This is comparable to the interaction energy between the ion

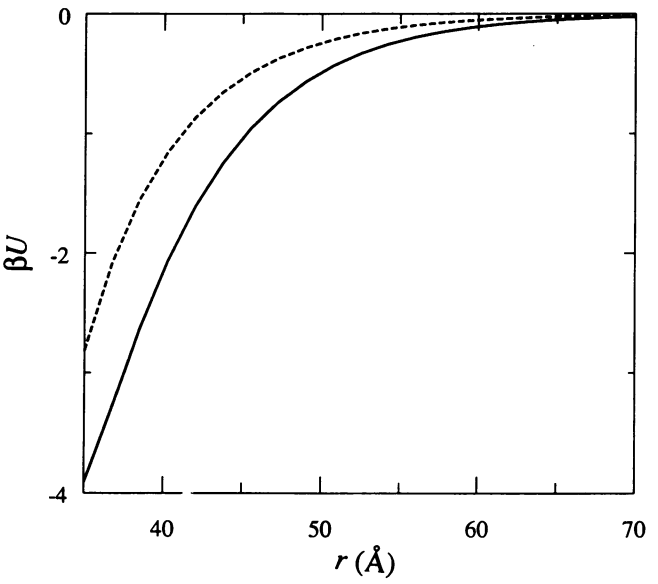

FIGURE 9 Comparison of the interaction potential when cytochrome *c* is treated as a region of low dielectric constant and excluding ions (*solid curve*) or as three test charges (*dashed curve*). The solid curve is the same as in Fig. 6.

and a central charge of 10e in the protein, which is $0.37k_BT$ from Eq. 59. For smaller ions or ions that bear more charges U_{sm} is even larger. The consequence of neglecting this contribution in studying ionic ligand binding to proteins (e.g., in reference 4) has to be assessed.

It is interesting to make a connection between our approach to the protein–protein diffusional association rate constant and the approach of Doi (27) and Temkin and Yakobson (20). Both approaches can be cast into the following simple chemical scheme

$$\text{separate reactants} \underset{k_{-1}}{\overset{k_1}{\rightleftarrows}} \text{reaction complex} \xrightarrow{\tau^{-1}} \text{product}. \quad (61)$$

The association rate constant of the scheme is easily obtained by making the steady-state approximation for the reaction complex,

$$k(\infty) = \frac{k_1}{k_{-1} + \tau^{-1}}\,\tau^{-1}. \quad (62)$$

Noting that $k_1/k_{-1} = \int_{\mathbf{x}\in\Gamma} d\mathbf{x} P_{eq}(\mathbf{x}) = \langle e^{-\beta U}\rangle_\Gamma \nu_\Gamma$ where $\nu_\Gamma = (4\pi)^{-2}\int_{\mathbf{x}\in\Gamma} d\mathbf{x}$ is the volume of the reaction region Γ, we can rearrange Eq. 62 into the form

$$k(\infty) = \langle e^{-\beta U}\rangle_\Gamma \frac{\nu_\Gamma k_{-1}\nu_\Gamma\tau^{-1}}{\nu_\Gamma k_{-1} + \nu_\Gamma\tau^{-1}}. \quad (63)$$

The inverse of k_{-1} in the chemical scheme of Eq. 61 can be identified as the mean total residence time of the reaction complex against diffusion. This is exactly the quantity introduced by Doi (27) and calculated by Temkin and Yakobson (20) for two patched spheres when the interaction potential is absent. In our approach we simulate the frequent interconversion between the separate reactants and the reaction complex and the occasional conversion of the reaction complex to the product. The association rate constant is obtained from the distribution of the lifetimes of the reactants. A unique feature of our approach is that not only is the steady-state rate constant found, so is the whole time dependence of the association rate coefficient.

According to the chemical scheme, if $k_{-1} \gg \tau^{-1}$ we obtain $k(\infty) \approx \langle e^{-\beta U}\rangle_\Gamma \nu_\Gamma \tau^{-1} = k(0)$, a quantity that is proportional to the average Boltzmann factor $\langle e^{-\beta U}\rangle_\Gamma$ but independent of diffusion. On the other hand, if $k_{-1} \ll \tau^{-1}$ we obtain $k(\infty) \approx \langle e^{-\beta U}\rangle_\Gamma \nu_\Gamma k_{-1}$, the diffusion-controlled rate constant $k_D(\infty)$. If we still want $k(\infty)$ to be proportional to the average Boltzmann factor $\langle e^{-\beta U}\rangle_\Gamma$, k_{-1} has to be insensitive to the presence of the interaction potential. Specific calculations verify that this is indeed the case when the reaction region Γ is small (see, e.g., Eq. 23). In the context of the dimer assembly of human hemoglobin, Mrabet et al. (37) proposed a chemical scheme somewhat different from Eq. 61, but arrived at the same conclusion about the scaling of $k(\infty)$ with $\langle e^{-\beta U}\rangle_\Gamma$.

Up to this point we have considered only the situation that the conversion from the reaction complex to the product is irreversible. However, reversibility can be easily taken into account in our model. Suppose that the product $[P]$ is converted into the reaction complex with a rate constant $(\tau_p)^{-1}$; then the rate equation (38)

$$\frac{d[1]}{dt} = \frac{k(t)}{k(0)}\{-k(0)[1][2] + \tau_p^{-1}[P]\} \quad (64)$$

describes the reversible situation to a good approximation. As usual we have assumed that the concentration [2] of one protein is much higher than the concentration [1] of the other. Hence, once we obtain the time-dependent rate coefficient $k(t)$ for the irreversible situation, we can put it into Eq. 64 to study the effect of reversibility.

The main shortcoming of our protein–protein diffusional association model is in the use of spheres to represent irregularly shaped proteins. This is necessitated by the ability to solve the Poisson–Boltzmann equation. Despite this shortcoming it has produced fruitful results, as summarized above. The consequence of putting realistic charge distributions rather than three representative charges in the model will be studied and the possibility of using nonspherical models will be explored in the future.

APPENDIX A

In this appendix we use the constant-flux approximation to derive the time-dependent rate coefficient of two patched spheres that are undergoing translational and rotational diffusion under the influence of a centrosymmetric interaction potential.

The relevant problem to solve is Eqs. 1–2 subject to the boundary condition of Eq. 3 on the spherical surface $r = a$. Initially the distribution function $P = P(r\mathbf{e}, \mathbf{e}_1, \mathbf{e}_2, t)$ takes the equilibrium distribution

$$P(t=0) = P_{eq} = (4\pi)^{-2} e^{-\beta U(r)}. \quad \text{(A1)}$$

At infinite separation, P stays at its initial value,

$$P(r=\infty) = (4\pi)^{-2}. \quad \text{(A2)}$$

It can be easily checked that P_{eq} is a particular solution that satisfies both the initial condition (Eq. A1) and the outer boundary condition (Eq. A2). By making

$$P = P_{eq} + P_1, \quad \text{(A3)}$$

we have in P_1 a solution that has zero initial and outer boundary values. The inner boundary condition (Eq. 3) is of course satisfied by $P_{eq} + P_1$.

To proceed we make the ansatz

$$P_1 = e^{-\beta U(r)} \sum_{lml_1m_1l_2m_2} A(r, t; lml_1m_1l_2m_2) \times Y_{lm}(\theta, \phi) Y_{l_1m_1}(\theta_1, \phi_1) Y_{l_2m_2}(\theta_2, \phi_2). \quad \text{(A4)}$$

Inserting this into Eqs. 1–2 and taking the Laplace transform, we obtain

$$\left[\mathcal{L}^+(r) - (\mu_{l_1l_2}^2(s) + \frac{l(l+1)}{r^2})\right]\hat{A} = 0, \quad \text{(A5)}$$

where $\mu_{l_1l_2}(s) = [(D_1l_1(l_1+1) + D_2l_2(l_2+1) + s)/D]^{1/2}$. Let $f_l[r; \mu_{l_1l_2}(s)]$ be the regular solution of Eq. A5; then the Laplace transform of P_1 can be written as

$$\hat{P}_1 = e^{-\beta U(r)} \sum_{lml_1m_1l_2m_2} a_{lml_1m_1l_2m_2} f_l[r; \mu_{l_1l_2}(s)] \times Y_{lm}(\theta, \phi) Y_{l_1m_1}(\theta_1, \phi_1) Y_{l_2m_2}(\theta_2, \phi_2). \quad \text{(A6)}$$

The crucial step to determine the remaining set of constants is to approximate the radiation boundary condition in Eq. 3 by requiring that the flux is a constant over the reactive patch,

$$De^{-\beta U(a)}\left[\frac{\partial}{\partial r} e^{\beta U(r)} \hat{P}\right]_{r=a} = u_1(\gamma_1)u_2(\gamma_2)e^{-\beta U(a)} \frac{Q(s)}{s}, \quad \text{(A7)}$$

and that the radiation boundary condition is satisfied on the average,

$$\iiint d\mathbf{e}\, d\mathbf{e}_1\, d\mathbf{e}_2 u_1(\gamma_1)u_2(\gamma_2)e^{-\beta U(a)} \frac{Q(s)}{s} = \kappa \iiint d\mathbf{e}\, d\mathbf{e}_1\, d\mathbf{e}_2 u_1(\gamma_1)u_2(\gamma_2)\hat{P}(r=a). \quad \text{(A8)}$$

To make use of Eqs. A7 and A8, we need to express $u_i(\gamma_i)$ in terms of spherical harmonics of $\mathbf{e}$, $\mathbf{e}_1$, and $\mathbf{e}_2$. They are (39)

$$u_i(\gamma_i) = \sum_{l_im_i} (-1)^{(i-1)l_i} c_i(l_i) Y^*_{l_im_i}(\theta, \phi) Y_{l_im_i}(\theta_i, \phi_i), \quad \text{(A9)}$$

where

$$c_i(l_i) = 2\pi \int_0^\pi u_i(\gamma_i) P_{l_i}(\cos\gamma_i) \sin\gamma_i d\gamma_i. \quad \text{(A10)}$$

Now, multiplying both sides of Eq. A7 by $Y^*_{lm}(\theta, \phi) \times Y^*_{l_1m_1}(\theta_1, \phi_1) Y^*_{l_2m_2}(\theta_2, \phi_2)$ and integrating over $\mathbf{e}$, $\mathbf{e}_1$, and $\mathbf{e}_2$ by using Eq. A9, we find

$$a_{lml_1m_1l_2m_2} = \frac{(-1)^{l_2} Q(s) c_1(l_1) c_2(l_2)}{sDf_l'[a; \mu_{l_1l_2}(s)]} B^*_{lml_1m_1l_2m_2}. \quad \text{(A11)}$$

The B coefficients are

$$B_{lml_1m_1l_2m_2} = \int d\mathbf{e} Y_{lm}(\theta, \phi) Y_{l_1m_1}(\theta, \phi) Y_{l_2m_2}(\theta, \phi), \quad \text{(A12)}$$

or, in terms of 3-j symbols (39),

$$B_{lml_1m_1l_2m_2} = \left[\frac{(2l_1+1)(2l_2+1)(2l+1)}{4\pi}\right]^{1/2} \times \begin{pmatrix} l_1 & l_2 & l \\ 0 & 0 & 0 \end{pmatrix} \begin{pmatrix} l_1 & l_2 & l \\ m_1 & m_2 & m \end{pmatrix}. \quad \text{(A13)}$$

On the other hand, Eq. A8 can be evaluated to give

$$4\pi Q(s) c_1(0) c_2(0) = \frac{\kappa}{4\pi} c_1(0) c_2(0) + \kappa s \sum_{lml_1m_1l_2m_2} a_{lml_1m_1l_2m_2} f_l[a; \mu_{l_1l_2}(s)] \times (-1)^{l_2} c_1(l_1) c_2(l_2) B_{lml_1m_1l_2m_2}. \quad \text{(A14)}$$

From Eqs. A11 and A14, we obtain

$$Q(s) = \frac{D\kappa c_1(0)c_2(0)/4\pi}{4\pi D c_1(0)c_2(0) - \kappa \sum_{lml_1m_1l_2m_2} \frac{f_l[a; \mu_{l_1l_2}(s)]}{f_l'[a; \mu_{l_1l_2}(s)]} [c_1(l_1)c_2(l_2)]^2 |B_{lml_1m_1l_2m_2}|^2}. \quad \text{(A15)}$$

The sums over m, m_1, and m_2 can be evaluated, leading to

$$Q(s) = \frac{D\kappa c_1(0)c_2(0)/4\pi}{4\pi D c_1(0)c_2(0) - \kappa \sum_{ll_1l_2} \frac{f_l[a; \mu_{l_1l_2}(s)]}{f_l'[a; \mu_{l_1l_2}(s)]} [c_1(l_1)c_2(l_2)]^2 C_{ll_1l_2}}, \quad \text{(A16)}$$

where

$$C_{ll_1l_2} = \frac{(2l_1+1)(2l_2+1)(2l+1)}{4\pi} \begin{pmatrix} l_1 & l_2 & l \\ 0 & 0 & 0 \end{pmatrix}^2. \quad \text{(A17)}$$

As the time-dependent rate coefficient is just the total flux across the boundary $r = a$, this finally gives the expression in Eq. 6.

APPENDIX B

In this appendix we derive formulas for propagating a Brownian system in its configuration space $\mathbf{x} = (\mathbf{r}, \mathbf{e}_1, \mathbf{e}_2)$ in small time steps. The system, described by Eq. 42 with the sink term absent, consists of two spheres undergoing translational and rotational diffusion that have an intersphere displacement $\mathbf{r}$ and have unit vectors $\mathbf{e}_1$ and $\mathbf{e}_2$ attached. The system is under the influence of an interaction potential that depends on $\mathbf{r}$, $\mathbf{e}_1$, and $\mathbf{e}_2$.

To propagate the system in $\mathbf{x} = (\mathbf{r}, \mathbf{e}_1, \mathbf{e}_2)$ space in small time steps, one needs to pick configurations from the short-time Green function of the equation

$$\frac{\partial G_0}{\partial t} = \mathcal{L}_{tr} G_0, \quad \text{(B1a)}$$

$$\mathcal{L}_{tr} = D\nabla \cdot e^{-\beta U}\nabla e^{\beta U} + \sum_{i=1}^{2} D_i \Omega_i \cdot e^{-\beta U}\Omega_i e^{\beta U}. \quad \text{(B1b)}$$

To this end we note that the short-time Green function of the general equation of the form

$$\frac{\partial G_0}{\partial t} = -\frac{\partial}{\partial \mathbf{x}} \cdot \mathbf{A}(\mathbf{x}) G_0 + \frac{\partial}{\partial \mathbf{x}} \frac{\partial}{\partial \mathbf{x}} : \mathbf{B}(\mathbf{x}) G_0 \quad \text{(B2)}$$

is (40)

$$G_0(\mathbf{x}, \Delta t | \mathbf{x}_0, 0) = \left[1 - \frac{\partial}{\partial \mathbf{x}} \cdot \mathbf{A}(\mathbf{x}_0)\Delta t + \frac{\partial}{\partial \mathbf{x}} \frac{\partial}{\partial \mathbf{x}} : \mathbf{B}(\mathbf{x}_0)\Delta t + O(\Delta t^2)\right] \delta(\mathbf{x} - \mathbf{x}_0) \quad \text{(B3a)}$$

$$\approx \exp\left[-\frac{\partial}{\partial \mathbf{x}} \cdot \mathbf{A}(\mathbf{x}_0)\Delta t + \frac{\partial}{\partial \mathbf{x}} \frac{\partial}{\partial \mathbf{x}} : \mathbf{B}(\mathbf{x}_0)\Delta t\right] \delta(\mathbf{x} - \mathbf{x}_0). \quad \text{(B3b)}$$

If the inverse of the matrix $\mathbf{B}(\mathbf{x}_0)$ exists, Eq. B3b reduces to (N: dimension of $\mathbf{x}$)

$$G_0(\mathbf{x}, \Delta t | \mathbf{x}_0, 0) = (4\pi\Delta t)^{-N/2} \{\det [\mathbf{B}(\mathbf{x}_0)]\}^{1/2} \times \exp\{-[\mathbf{x} - \mathbf{x}_0 - \mathbf{A}(\mathbf{x}_0)\Delta t]^{\mathrm{T}} \cdot [\mathbf{B}(\mathbf{x}_0)]^{-1} \times [\mathbf{x} - \mathbf{x}_0 - \mathbf{A}(\mathbf{x}_0)\Delta t]/(4\Delta t)\}. \quad \text{(B4)}$$

To order Δt all the three distributions of Eqs. B3a–4 are produced by generating $\mathbf{x}$ by

$$\mathbf{x} = \mathbf{x}_0 + \mathbf{A}(\mathbf{x}_0)\Delta t + \mathbf{C}\sqrt{2\Delta t}, \quad \text{(B5)}$$

where $\mathbf{C}$ is a vector of Gaussian random numbers with the following properties:

$$\langle \mathbf{C} \rangle = 0, \quad \text{(B6a)}$$

$$\langle \mathbf{C}\mathbf{C}^{\mathrm{T}} \rangle = \mathbf{B}(\mathbf{x}_0). \quad \text{(B6b)}$$

Note that Eqs. B5–6b propagate the system described by Eq. B2 even when the inverse of $\mathbf{B}(\mathbf{x}_0)$ does not exist.

The operator $\mathcal{L}_{tr}$ of Eq. B1b can be cast into the form in Eq. B2,

$$\mathcal{L}_{tr} = \frac{\partial}{\partial \mathbf{r}} \cdot (D\beta\nabla U) + \frac{\partial}{\partial \mathbf{r}} \frac{\partial}{\partial \mathbf{r}} : D\mathbf{1} + \sum_{i=1}^{2} \left\{ D_i \frac{\partial}{\partial \mathbf{e}_i} \cdot \left[(\mathbf{e}_i \cdot \mathbf{e}_i)\beta \frac{\partial U}{\partial \mathbf{e}_i} - \left(\mathbf{e}_i \cdot \beta \frac{\partial U}{\partial \mathbf{e}_i}\right)\mathbf{e}_i + 2\mathbf{e}_i \right] + D_i \frac{\partial}{\partial \mathbf{e}_i} \frac{\partial}{\partial \mathbf{e}_i} : [(\mathbf{e}_i \cdot \mathbf{e}_i)\mathbf{1} - \mathbf{e}_i\mathbf{e}_i] \right\}, \quad \text{(B7)}$$

where $\mathbf{1}$ is the unit matrix. Consequently, the formulas for generating $\mathbf{r}$ and $\mathbf{e}_i$ are

$$\mathbf{r} = \mathbf{r}_0 - (\beta\nabla U)D\Delta t + \mathbf{C}\sqrt{2D\Delta t}, \quad \text{(B8a)}$$

$$\mathbf{e}_i = \mathbf{e}_{i0} - \left[2\mathbf{e}_{i0} + \beta \frac{\partial U}{\partial \mathbf{e}_{i0}} - \left(\mathbf{e}_{i0} \cdot \beta \frac{\partial U}{\partial \mathbf{e}_{i0}}\right)\mathbf{e}_{i0}\right] D_i \Delta t + (\mathbf{1} - \mathbf{e}_{i0}\mathbf{e}_{i0})\mathbf{C}_i\sqrt{2D_i\Delta t}, \quad \text{(B8b)}$$

where $\mathbf{C}$ and $\mathbf{C}_i$ are $\mathbf{C}$ of Eqs. B6 with $\mathbf{B}(\mathbf{x}_0)$ identified with the unit matrix. To ensure unity of $\mathbf{e}_i$, they have to be normalized after each step. Eq. B8a for translational diffusion has been derived previously by Ermak and McCammon (41). The rotational diffusion algorithm, Eq. B8b, appears to be new. It has been used without derivation in studying the dielectric properties of a Brownian dipole lattice just recently (42).

I thank Attila Szabo and Robert Zwanzig for helpful discussions.

Received for publication 14 December 1992 and in final form 16 February 1993.

REFERENCES

1. Smoluchowski, M. V. 1917. Versuch einer mathematischen theorie der koagulationskinetik kolloider losungen. *Z. Phys. Chem.* 92:129–168.
2. Debye, P. 1942. Reaction rates in ionic solutions. *Trans. Electrochem. Soc.* 82:265–272.
3. Debye, P., and E. Huckel. 1923. Zur theorie der elektrolyte. *Phys. Z.* 24:185–206.
4. Sharp, K., R. Fine, K. Schulten, and B. Honig. 1987. Brownian dynamics simulation of diffusion to irregular bodies. *J. Phys. Chem.* 91:3624–3631.
5. Northrup, S. H., S. A. Allison, and J. A. McCammon. 1984. Brownian dynamics simulation of diffusion-influenced bimolecular reactions. *J. Chem. Phys.* 80:1517–1524.
6. Warwicker, J., and H. C. Watson. 1982. Calculation of the electric potential in the active site cleft due to α-helix dipoles. *J. Mol. Biol.* 157:671–679.
7. Davis, M. E., and J. A. McCammon. 1990. Electrostatics in biomolecular structure and dynamics. *Chem. Rev.* 90:509–521.
8. Northrup, S. H., J. O. Boles, and J. C. L. Reynolds. 1987. Electrostatic effects in the Brownian dynamics of association and orientation of heme proteins. *J. Phys. Chem.* 91:5991–5998.
9. Scatchard, G., and J. G. Kirkwood. 1932. Das verhalten von zwitterionen und von mehrwertigen ionen mit weit entfernten ladungen in electrolytlosungen. *Phys. Z.* 33:297–300.
10. Kirkwood, J. G. 1934. Theory of solutions of molecules containing widely separated charges with special application to zwitterions. *J. Chem. Phys.* 2:351–361.
11. Tanford, C., and J. G. Kirkwood. 1957. Theory of protein titration curves. I. General equations for impenetrable spheres. *J. Am. Chem. Soc.* 79:5333–5339.
12. Shire, S. J., G. I. H. Hanania, and F. R. N. Gurd. 1974. Electrostatic effects in myoglobin. Hydrogen ion equilibria in sperm whale ferrimyoglobin. *Biochemistry.* 13:2967–2974.
13. Matthew, J. B. 1985. Electrostatic effects in proteins. *Annu. Rev. Biophys. Biophys. Chem.* 14:387–417.
14. Weber, P. C., and G. Tollin. Electrostatic interactions during electron transfer reactions between *c*-type cytochromes and flavodoxin. *J. Biol. Chem.* 260:5568–5573.
15. Zhou, H.-X. 1990. Kinetics of diffusion-influenced reactions studied by Brownian dynamics. *J. Phys. Chem.* 94:8794–8800.
16. Shoup, D., G. Lipari, and A. Szabo. 1981. Diffusion-controlled bimolecular reaction rates. The effect of rotational diffusion and orientation constraints. *Biophys. J.* 36:697–714.
17. Solc, K., and W. H. Stockmayer. 1971. Kinetics of diffusion-controlled reaction between chemically asymmetric molecules. I. General theory. *J. Chem. Phys.* 54:2981–2988.
18. Solc, K., and W. H. Stockmayer. 1973. Kinetics of diffusion-controlled reaction between chemically asymmetric molecules. II. Approximate steady-state solution. *Int. J. Chem. Kinet.* 5:733–752.

19. Szabo, A., D. Shoup, S. H. Northrup, and J. A. McCammon. 1982. Stochastically gated diffusion-influenced reactions. *J. Chem. Phys.* 77:4484–4493.
20. Temkin, S. I., and B. I. Yakobson. 1984. Diffusion-controlled reactions of chemically anisotropic molecules. *J. Phys. Chem.* 88:2679–2682.
21. Berg, O. G. 1985. Orientation constraints in diffusion-limited macromolecular association. The role of surface diffusion as a rate-enhancing mechanism. *Biophys. J.* 47:1–14.
22. Northrup, S. H., J. C. L. Reynolds, C. M. Miller, K. J. Forrest, and J. O. Boles. 1986. Diffusion-controlled association rate of cytochrome *c* and cytochrome *c* peroxidase in a simple electrostatic model. *J. Am. Chem. Soc.* 108:8162–8170; 1987, 109:3176.
23. Kang, C. H.,D. L. Brautigan, N. Oshroff, and E. Margoliash. 1978. Definition of cytochrome *c* binding domains by chemical modification. *J. Biol. Chem.* 253:6502–6510.
24. Szabo, A. 1989. Theory of diffusion-influenced fluorescence quenching. *J. Phys. Chem.* 93:6929–6939.
25. Zhou, H.-X., and A. Szabo. 1990. Mean field theory of transient fluorescence quenching in the frequency domain. *J. Chem. Phys.* 92:3874–3880.
26. Wilemski, G., and M. Fixman. 1973. General theory of diffusion-controlled reactions. *J. Chem. Phys.* 58:4009–4019.
27. Doi, M. 1975. Theory of diffusion-controlled reaction between non-simple molecules. *Chem. Phys.* 11:107–113, 115–121.
28. Press, W. H., B. P. Flannery, S. A. Teukolsky, and W. T. Vetterling. 1986. Numerical Recipes. Cambridge University Press, Cambridge, UK. 818 pp.
29. Luty, B. A., J. A. McCammon, and H.-X. Zhou. 1992. Diffusive reaction rates from Brownian dynamics simulations: replacing the outer cutoff surface by an analytical treatment. *J. Chem. Phys.* 97:5682–5686.
30. Jackson, J. D. 1962. Classical Electrodynamics. John Wiley & Sons Inc., New York. 641 pp.
31. McCartney, L. N., and S. Levine. 1969. An improvement on Derjaguin's expression at small potentials for the double layer interaction energy of two spherical colloidal particles. *J. Colloid Interface Sci.* 30:345–354.
32. Northrup, S. H., and H. P. Erickson. 1992. Kinetics of protein–protein association explained by Brownian dynamics computer simulation. *Proc. Natl. Acad. Sci. USA.* 89:3338–3342.
33. Gardiner, C. W. 1985. Handbook of Stochastic Methods. 2nd ed. Springer-Verlag, Berlin. 442 pp.
34. Lamm, G., and K. Schulten. 1983. Extended Brownian dynamics. II. Reactive, nonlinear diffusion. *J. Chem. Phys.* 78:2713–2734.
35. Stehfest, H. 1970. Numerical inversion of Laplace transforms. *Comm. of the ACM.* 13:47–49.
36. Corin, A. F., G. McLendon, Q. Zhang, R. A. Hake, J. Falvo, K. S. Lu, R. B. Ciccarelli, and D. Holzschu. 1991. Effects of surface amino acid replacements in cytochrome *c* peroxidase on complex formation with cytochrome *c*. *Biochemistry.* 30:11585–11595.
37. Mrabet, N. T., M. J. McDonald, S. Turci, R. Sarkar, A. Szabo, and H. F. Bunn. 1986. Electrostatic attraction governs the dimer assembly of human hemoglobin. *J. Biol. Chem.* 261:5222–5228.
38. Szabo, A. 1991. Theoretical approaches to reversible diffusion-influenced reactions: monomer–excimer kinetics. *J. Chem. Phys.* 95:2481–2490.
39. Zare, R. N. 1988. Angular Momentum. John Wiley & Sons Inc., New York. 349 pp.
40. Risken, H. 1984. The Fokker-Planck Equation. Springer-Verlag, Berlin. 454 pp.
41. Ermak, D. L., and J. A. McCammon. 1978. Brownian dynamics with hydrodynamic interactions. *J. Chem. Phys.* 69:1352–1360.
42. Zhou, H.-X., and B. Bagchi. 1992. Dielectric and orientational relaxation in a Brownian dipolar lattice. *J. Chem. Phys.* 97:3610–3620.